Talanta 234 (2021) 122643

Contents lists available at ScienceDirect

Talanta

journal homepage: www.elsevier.com/locate/talanta

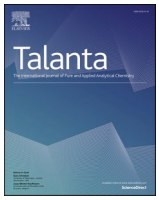

Amplified electrochemical biosensing based on bienzymatic cascade catalysis confined in a functional DNA structure

Jiaxi Gao [a], Xiaoyu Hua [a], Ruo Yuan [a], Qiong Li [b,**], Wenju Xu [a,*]

[a] Key Laboratory of Luminescence Analysis and Molecular Sensing (Southwest University), Ministry of Education, School of Chemistry and Chemical Engineering, Southwest University, Chongqing, 400715, China
[b] College of Geophysics, Chengdu University of Technology, Chengdu, 610059, China

ARTICLE INFO

Keywords:
Electrochemical biosensor
Bienzymatic cascade catalysis
Glucose oxidase
Horseradish peroxidase
Functional DNA structure

ABSTRACT

Herein, an amplified and renewable electrochemical biosensor was developed via bienzymatic cascade catalysis of glucose oxidase (GOx) and horseradish peroxidase (HRP), which were confined in a functional Y-shaped DNA nanostructure oriented by a dual-thiol-ended hairpin probe (dSH-HP) with a paired stem as a rigid scaffold and unpaired loop as enclosed binding platform. For proof-of-concept assay of sequence-specific biomarker DNA related to Alzheimer's disease (aDNA), GOx and redox ferrocene-modified HRP (Fc@HRP) were chemically conjugated in two enzyme strands (GOx-ES1 and Fc@HRP-ES2), respectively. The repeated recycling of aDNA was powered by the displacement of GOx-ES1 by aDNA and exonuclease III (ExoIII)-assisted cleavage reaction for amplified output of numerous GOx-ES1 as dependent transducers, together with Fc@HRP-ES2 which was simultaneously hybridized with dSH-HP to assemble this DNA structure. Rationally, the bienzymatic cascade catalysis was motivated through GOx-catalyzed glucose oxidization to in situ generate hydrogen peroxide (H_2O_2) and overlapped HRP-catalyzed H_2O_2 decomposition to promote the electron transfer, producing significantly enhanced electrochemical signal of Fc with an ultrahigh sensitivity down to 0.22 fM of aDNA. Benefited from the unique design of dSH-HP-oriented bienzymatic cascades, this one-step strategy without non-specific blockers passivation was simple and renewable, and would pave a promising avenue for sensitive electrochemical assay of biomolecules.

1. Introduction

Most biochemical processes occurred efficiently and specifically in vivo are implemented and mediated by a series of enzyme reactions, which depended on the appropriate spatial arrangement of multiple enzymes [1–3]. Enzymatic cascade reaction, as an efficient signal amplification tool, has been widely used for the highly sensitive detection of nucleic acids, proteins, ions or others [4–7]. In a typical case, the reaction product of one enzyme can be used as a catalytic substrate for another enzyme [4,5]. Currently, great efforts have been made to investigate the distance dependency of enzyme cascade catalysis [8,9]. Once the enzymes are organized in an appropriate distance, the cascade reaction can generate efficient mass transfer and increase the local concentration of substrates, thereby resulting in high catalytic efficiency of enzyme cascade reaction [10]. For example, glucose oxidase (GOx) firstly catalyzes glucose to generate gluconic acid and hydrogen peroxide (H_2O_2), and H_2O_2, as the substrate of horseradish peroxidase (HRP), can be further catalytically reduced into H_2O [11]. As HRP has a much higher turnover rate than GOx, the diffusion distance of H_2O_2 will be a critical factor influencing the rate of this enzyme cascade catalysis [1]. Our group has already done several interesting works on the enzyme cascade systems [12–14]. For instance, a distance-controllable DNA tweezer was designed to dynamically regulate the interenzyme spacing for efficient enzyme cascade amplification [12]. However, the reaction was totally taken place in a homogeneous solution without any separation operation, resulting in high electrochemical background signal. Inevitably, the real detection for targeting analytes at ultralow level was limited. Also, a rigid DNA tetrahedron scaffold was developed to regulate the distance of interenzymes in a cascade system, where the uncertainty of GOx or HRP catalysis easily caused false-positive signals [13]. Therefore, it is significant to explore a new enzyme cascade-based strategy by improving the catalysis efficiency to minimize false-positive

* Corresponding author.
** Corresponding author.
E-mail addresses: liqiong@cdut.cn (Q. Li), 1572808690@qq.com (W. Xu).

https://doi.org/10.1016/j.talanta.2021.122643
Received 8 May 2021; Received in revised form 12 June 2021; Accepted 20 June 2021
Available online 3 July 2021

background signal.

In biological researches, DNA nanomaterials are considered as excellent materials for signal translation, biosensing, enzyme immobilization, and et al., because of good biocompatibility, high specificity, structure controllability and sequence programmability [15–17]. Versatile DNA nanomaterials with unique structural features have been applied for the accurate quantification of targeting molecules, or even cell imaging in biosensing systems, such as i-motif, DNA tetrahedron, and hairpin DNA [18–23]. Among them, functional Y-shaped DNA nanostructures have been widely used in the construction of biosensors [24–26]. For example, by simply adding two kinds of sequence-specific DNA probes to interact with the targeting DNA strand, a functional Y-shaped DNA structure was assembled, with which a sensitive biosensor was successfully developed, achieving fast and low-cost detection [26]. In the other hand, stem-loop-structured DNA hairpins labeled with thiol (-SH) or amino (-NH_2) have been used as fascinating recognizable elements for constructing electrochemical biosensors [27–29]. As reported by Li and his co-workers, a dually –SH–ended hairpin as a capture probe could be rapidly and robustly assembled on a modified electrode surface and kept proper upright orientation conformation. As such, the proposed biosensor showed a highly specific recognition to the targeting molecule, as well as an impressive ability to suppress background signal [27]. In the dual –SH–labeled hairpin DNA, the paired stem acted as a rigid scaffold to keep it upright conformation, while the unpaired loop could provide diversity of constructing an enclosed platform with more modification or binding sites, particularly the guided conjugation or immobilization of multienzymes. By integrated with this, a functional Y-shaped DNA structure was assembled to enable one-step modification of electrode with simplification and convenience.

Based on bienzymatic cascade catalysis confined in a functional DNA structure oriented by a dual-SH hairpin probe (dSH-HP), an amplified electrochemical biosensor was developed to quantify Alzheimer's disease biomarker DNA (aDNA). To this end, bienzymes GOx and ferrocene (Fc)-modified HRP were chemically conjugated in two enzyme strands (GOx-ES1 and Fc@HRP-ES2), respectively. Using magnetic Au@Fe_3O_4 composites as substrate, the input aDNA was dependently translated into numerous GOx-ES1 output through exonuclease III (ExoIII)-assisted cleavage recycles of aDNA. The output GOx-ES1 together with Fc@HRP-ES2 was captured by dSH-HP, assembling this Y-shaped structure to orient the cascade catalysis of GOx and HRP in the presence of glucose and oxygen. Glucose was catalyzed by GOx to in situ generate gluconic acid and H_2O_2, and resultantly H_2O_2, as the substrate of HRP, was further reduced into H_2O and oxygen. With this harmonization of cascade reactions, the electron transfer of Fc oxidization was greatly promoted, outputting significantly enhanced electrochemical signal. Without non-specific blocker passivation, this cascade-based electrochemical strategy was simple and renewable, and could pave a promising avenue for sensitive biosensing and bioanalysis.

2. Experimental

2.1. Reagents and chemicals

Magnetic surface-aminated Fe_3O_4 microspheres (Fe_3O_4) were purchased from BaseLine ChromTech Research Centre (Tianjin, China). Mercaptohexanol (MCH), carboxylated ferrocene (Fc), chloroauric acid ($HAuCl_4{\cdot}4H_2O$), dithiothreitol (DTT), glucose, N-(3-(dimethylamino) propyl)-N′-ethylcarbodiimide hydrochloride (EDC), N-hydroxysulfosuccinimide (NHS), N-succinimidyl-3-(2-pyridyldithio) propionate (SPDP), and hexaammineruthenium (III) chloride ($[Ru(NH_3)_6]^{3+}$, RuHex) were obtained from Sigma-Aldrich (St. Louis, MO, USA). J&K Chemical Technology Co., Ltd. (Beijing, China) provided us with GOx, HRP, and tris (hydroxymethyl) aminomethane hydrochloride (Tris-HCl) (pH 7.4). ExoIII and all HPLC-purified oligonucleotides were purchased from Sangon Biotech Co. Ltd (Shanghai, China), and Table S1 illustrated the detailed base sequence. 0.1 M phosphate-buffered saline (PBS, pH 7.2) containing KH_2PO_4, Na_2HPO_4, NaCl and KCl was obtained from Beijing Dingguo Changsheng Biotechnology Co. Ltd (Beijing, China), which was adjusted to pH 7.0 by adding HCl as the working solution.

2.2. Apparatus

By using a conventional three-electrode system with a glassy carbon electrode (GCE, in 4 mm diameter) as the working electrode, a saturated calomel electrode (SCE) as the reference electrode ($E^{\theta} = +0.2412$ V), and a platinum wire as the auxiliary electrode, the CHI 760 E electrochemistry workstation (Shanghai Chenhua Instruments Co., Ltd., China) was to monitor cyclic voltammetry (CV), electrochemical impedance spectroscopy (EIS) and square wave voltammetry (SWV) of the developed electrodes. Polyacrylamide gel electrophoresis (PAGE) of different samples in a loading buffer containing 8% nondenaturing polyacrylamide gel was conducted in a DYY-8C electrophoretic apparatus (Beijing, Wo De Life Sciences Instrument Co., Ltd., China) at 120 V for 80 min in 1 × TBE buffer (pH 8.0), and after stained with ethidium bromide (EB) the gel images were taken by an imaging system (Hercules, CA, USA) under UV light illumination. The morphology of prepared nanomaterials was tracked by using scanning electron microscopy (SEM, S-4800, Hitachi, Tokyo, Japan) at a voltage of 20 kV and the transmission electron microscope (TEM, H600, Hitachi, Japan). The X-ray photoelectron spectroscopy (XPS) was carried out by VG Scientific ESCALAB 250 spectrometer (Thermoelectricity Instruments, USA). UV–visible (UV–Vis) spectrum (UV-2501 PC Spectrometer, Shimadzu, Japan) recorded in the range from 350 nm to 750 nm. Scanning electron micrograph (SEM) was obtained by the scanning electron microscope (SEM, S-4800, Hitachi, Japan).

2.3. Modification and conjugation of GOx-ES1 and Fc@HRP-ES2

Each 200 μL of enzyme strand 1 (ES1) with 4 bases of T (T_4) close to 3' terminus and enzyme strand 2 (ES2) (4 μM) were separately pretreated with DTT (1 μL, 10 M) for 2 h to avoid the formation of S–S bonds. After 0.5 mg carboxylated Fc was dissolved in 100 μL PBS (pH 7.2) containing 10 mM NHS and 40 mM EDC for 1 h to activate –COOH groups, 100 μL HRP (2 μM) was added and kept at room temperature for 4 h, allowing the conjunction of Fc and HRP (Fc@HRP) via –COOH and –NH_2 combination. When 200 μL of GOx (1 μM) or Fc@HRP was separately treated with 1 μL SPDP (4 M) for 2 h, followed by corresponding addition of the activated ES1 (200 μL, 4 μM) into GOx and ES2 (200 μL, 4 μM) into Fc@HRP. After 2 h, the products, GOx-ES1 and Fc@HRP-ES2, were obtained.

2.4. GOx-ES1 output by aDNA-activated ExoIII cleavage recycling

Briefly, Au nanoparticles (AuNPs) were prepared by quickly adding 0.5 mL sodium citrate (1%, *w/w*) in 100 mL boiled $HAuCl_4$ solution (1%, *w/w*) for keeping 15 min, followed by cooling down to ambient temperature. In 1 mL of the prepared AuNPs, 100 μL NH_2-modified Fe_3O_4 (0.5%, *w/w*) magnetic microspheres were added and sonicated for 20 min. After the resultant mixture was shaken overnight at 4 °C and then undergone repeated magnetic centrifugation and washing using PBS (pH 7.2) at least three times, the obtained Au@Fe_3O_4 sediment was collected and again re-dispersed in 1 mL PBS (pH 7.2). Next, 10 μL of Au@Fe_3O_4 was mixed with 100 μL helper strand (HS) (2 μM) and reacted overnight, allowing the binding of HS onto Au@Fe_3O_4 surface through Au–N bond. Upon treated with 20 μL MCH (0.5 mM) as non-specific absorption blockers for 1 h, 100 μL GOx-ES1 (2 μM) was added for another 2 h, within which the base pairing of HS and ES1 reached to equilibrium. Finally, 20 μL AD-biomarker DNA (aDNA) (1 pM) and 1 μL ExoIII (100 U) were introduced at 37 °C for 2 h, dependently releasing numerous GOx-ES1 as transducers. It should be noted that each step in the above process was followed by repeated magnetic separation and washing

using Tris-HCl (pH 7.4) at least three times. Likewise, we also used other GOx-ES1 to implement the above aDNA-activated ExoIII cleavage recycling for their dependent output. The magnetic substrate Au@Fe_3O_4 composites were characterized by recording TEM image, UV–Vis absorption spectra and XPS (Fig. S1).

2.5. Fabrication of the electrochemical biosensor

A bare glassy carbon electrode (GCE) with a diameter of 4 mm was cleaned by polishing using Al_2O_3 powder (0.3 and 0.05 μm), and sonicated in DI water and anhydrous ethanol, followed by the electrodeposition in $HAuCl_4$ solution (1%, *w/w*) at −0.2 V potential for 30 s (depAu/GCE). The SEM images of bare GCe and depAu/GCE were shown in Fig. S2. The next introduction of 10 μL dual-thiol hairpin probe (dSH-HP) (2 μM) for 100 min at room temperature led to its stable immobilization via dual Au–S bonds in the modified electrode surface (dSH-HP/depAu/GCE). Then, each 10 μL of the above-collected GOx-ES1 and Fc@HRP-ES2 (2 μM) was simultaneously incubated for 2 h (GOx-ES1+Fc@HRP-ES2/dSH-HP/depAu/GCE), allowing stable assembly of this Y-shaped DNA structure through the hybridization reaction with the unpaired loop of dSH-HP. This fabricated biosensor was stored at 4 °C for subsequent electrochemical measurements. Similarly, other electrodes with GOx-ES1 (ES1 tethering T_0, T_2, T_7 and T_{12}) instead of GOx-ES1 (ES1 tethering T_4) were also fabricated. Upon treated with 10 μL of the competitive strand (**C***) (2 μM) for 2 h, this developed electrode can be regenerated by dehybridizing GOx-ES1 from the "Y-shaped" DNA nanostructure. It should be noted that dSH-HP with 12 bp stem was firstly used, and others with 5, 8, 10 and 15 bp stem were used for control experiments.

2.6. Electrochemical measurements

To monitor the stepwise fabrication of the developed electrodes, both CV and EIS were measured in 5 mM $[Fe(CN)_6]^{3-/4-}$ (pH 7.4). CV curves were obtained in the potential range from −0.2 to 0.6 V with a scan rate of 100 mV s^{-1}, and EIS was performed with ac frequency from 10^{-1} to 10^5 Hz, excitation signal of 5 mV and formal potential of 220 mV. The SWV response of the proposed electrode in different conditions was scanned in PBS (pH 7.0) containing 4 mM glucose (optimized) from 0.1 V to 0.4 V potential. In all SWV plots, the difference (ΔI, μA) of the peak current at about +0.27 V (characteristic oxidation potential of Fc) *vs.* the Blank without aDNA in this system was used to investigate the analytical performances of our biosensor.

3. Results and discussion

3.1. Design of the electrochemical biosensor

To achieve rapid and reliable electrochemical detection of sequence-specific biomarker DNA, bienzymatic cascade catalysis confined in one-step assembled functional Y-shaped DNA structure would be desired to obtain high catalysis efficiency. In this typical cascade system (as shown in Scheme 1), GOx firstly catalyzed the oxidization of glucose in the presence of oxygen to in situ generate gluconic acid and H_2O_2. Resultantly, H_2O_2 as the substrate of HRP could be further catalytically reduced into H_2O and oxygen, cooperatively promoting the electron transfer of redox-active ferrocene (Fc) oxidation in response to the variable Alzheimer's disease biomarker DNA (aDNA) as a model. The reaction equations of cascade catalysis are schematically as follows [4,5,

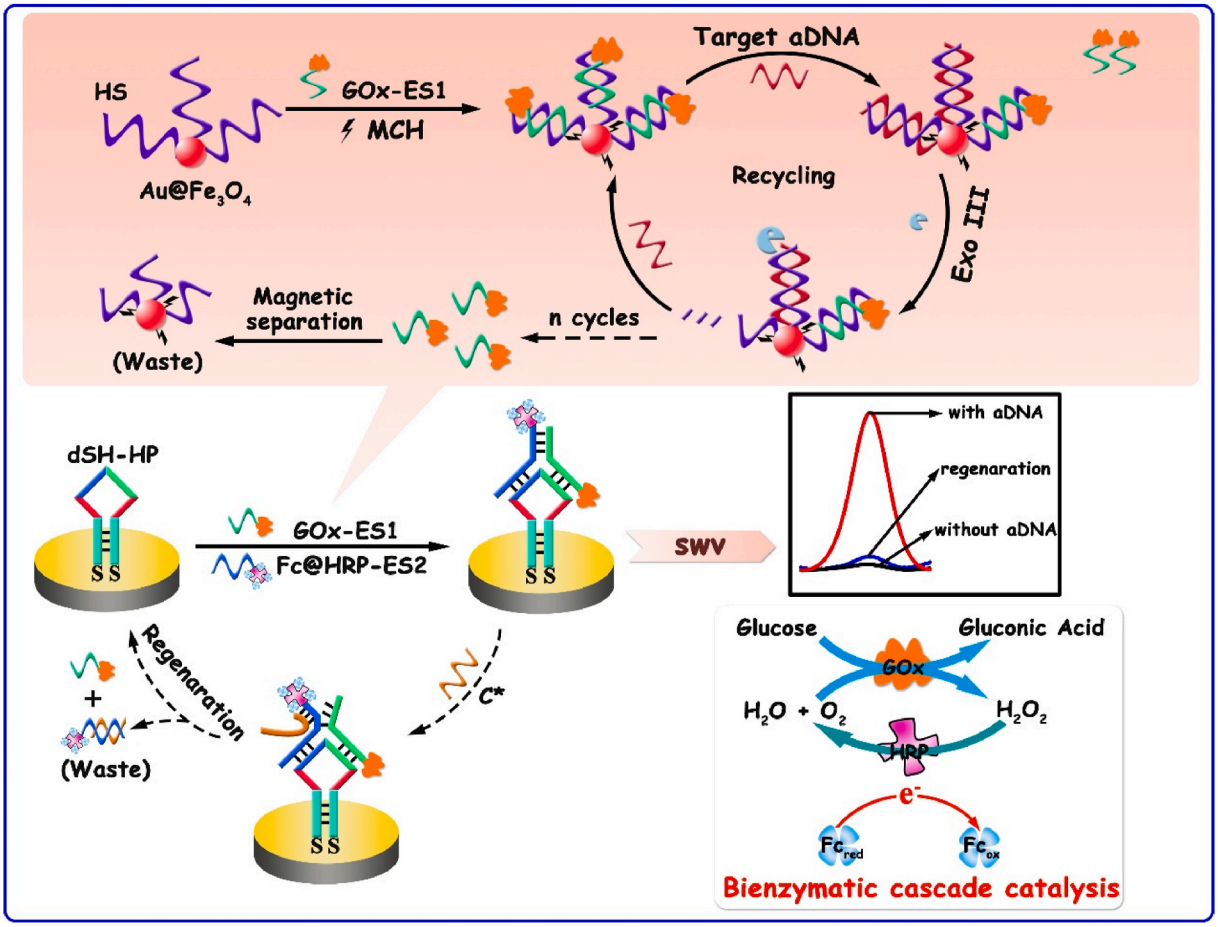

Scheme 1. Schematic diagrams of aDNA-activated ExoIII cleavage recycling for GOx-ES1 output, and fabrication of electrochemical biosensor with signal amplification implemented by bienzymatic cascade catalysis of GOx and HRP confined in dSH-HP-oriented functional Y-shaped structure.

11,12]:

Here, when the Fc-conjugated working electrode was scanned into positive potential from 0.1 V to 0.4 V, the oxidation of Fc_{red} into Fc_{ox} was driven to produce SWV signal. Concurrently, two cascade reactions catalyzed by GOx and HRP were initiated by glucose (GOx-catalyzed oxidation) added in the testing PBS solution, where the electron transfers (i.e. current) was overlapped with that of Fc oxidation, cooperatively enhancing the SWV signal. As a proof-of-concept, HRP was firstly modified with Fc (Fc@HRP), and then GOx and Fc@HRP were chemically conjugated in two enzyme strands (GOx-ES1 and Fc@ HRP-ES2). Prior to cascade amplification, the background interference of translating input aDNA into GOx-ES1 output was minimized by using magnetic Au@Fe_3O_4 as substrate (see Scheme 1A, where HS was initially combined in Au@Fe_3O_4 surface via Au–N bonds to hybridize with GOx-ES1. The subsequent presence of aDNA and ExoIII activated the repeated and progressive recycling of aDNA by displacing GOx-ES1 and ExoIII-recognizable cleavage of the formed duplex, achieving the aDNA-responsive output of numerous GOx-ES1 after stepwise magnetic centrifugation. Rationally, a dually –SH–ended hairpin probe (dSH-HP), which encoded a paired stem as a rigid scaffold and an unpaired loop as an enclosed binding platform, captured the output GOx-ES1 and Fc@HRP-ES2, stably orienting the structural function in the electrode surface. As expected, the confined GOx and HRP were able to provide the desired spatial distance for a highly efficient cascade reaction [12–14], greatly promoting the electron transfer of Fc oxidation in the sensing interface. Thus, the electrochemical signal was significantly enhanced to gain a high sensitivity of aDNA detection. Notably, by utilizing the upright dSH-HP with rigidity to orient GOx and HRP, this developed biosensor was simplified without non-specific blocker passivation and also renewable through the structure disassembling by a competitive strand (**C***) to take off Fc@HRP-ES2. Thus, the electrochemical strategy would pave a new avenue for convenient, specific and sensitive biosensing and bioanalysis. The PAGE image of different DNA samples was listed in Fig. S3.

3.2. Electrochemical characterization

CV and EIS of the stepwise fabrication of the electrochemical biosensor were conducted in $[Fe(CN)_6]^{3-/4-}$ (pH 7.4). Notably, to better understand the electrochemical response, the electrode was fabricated by using HRP-ES2 without conjugation of Fc in HRP. Obviously from Fig. 1A and B, we can see a pair of well-defined and reversible CV response for bare GCE (curve a), and increased CV signal and decreased electron-transfer resistance (R_{et}) in Nyquist plots (curve b) after electrodeposited in $HAuCl_4$ solution. But the incubation of non-conductive dSH-HP resulted in the decreasing of CV current and the increasing of EIS (curve c), and the same change for CV and EIS was also observed upon introducing GOx-ES1 and HRP-ES2 (curve d), revealing the simultaneous hybridization among dSH-HP, GOx-ES1 and HRP-ES2. As shown in the inset in Fig. 1B, the fitted Randle equivalent circuit corresponds to EIS curves included R_{et}, the ohmic resistance of the electrolyte solution (R_s), the capacitance (*CPE*) and the Warburg impedance (Z_w) [28].

To investigate the electrochemical readout of Fc conjugated in HRP-ES2 in response to aDNA, we compared the SWV signal of the electrode depAu/GCE before and after continuously modifying dSH-HP and Fc@HRP-ES2. As shown in Fig. 1C, almost no SWV response was observed in PBS (pH 7.0) containing glucose (4 mM) for depAu/GCE (curve b) and dSH-HP/depAu/GCE (curve c), because of the absence of electron mediator in the electrode surface. After introducing GOx-ES1 and Fc@HRP-ES2, the SWV current was significantly increased (curve e), suggesting the formation of Y-shaped structure with orienting GOx and HRP for cascade catalysis.

3.3. Electroactive surface area of depAu/GCE and dSH-HP-immobilized estimation

The stable immobilization of dSH-HP in the electrode surface has a substantial effect on the upright orientation of DNA structure to implement the highly efficient cascade reaction of GOx and HRP. This is directly dependent on the electroactive surface area (A, mm^2) after Au-electrodeposition in GCE (depAu/GCE). Based on the above observations, we firstly investigated the optimum base number of a paired stem of dSH-HP, as well as the binding time of dSH-HP, the reaction time of ExoIII, the glucose concentration in the electrolyte, and the incubation time of GOx-ES1 and Fc@HRP-ES2. Under the optimized experiment conditions (Fig. S4), the A of depAu/GCE was evaluated by measuring the CV response at different scan rates (v). As displayed in Fig. 2A, the CV current gradually increased with the rising of v, while the anodic peak current (I_p) was proportional to the square root of v ($v^{1/2}$) with a regression equation of $I_p(\mu A) = 693.7v^{1/2}+7.923$ and a correlation coefficient (r) of 0.9998. According to Randles-Sevcik equation ($I_p = 2.69 \times 10^5 AD^{1/2}n^{3/2}v^{1/2}c$, where D is the diffusion coefficient of 6.20×10^{-6} $cm^2 \cdot s^{-1}$ at 25 °C, n is the electron transfer number, and c is the concentration, 5 mM) [30,31]. So, the electroactive surface area A of depAu/GCE was calculated to be 20.7 mm^2, which was larger about 65% than the physical area of bare GCE with 4 mm of diameter (12.6 mm^2) after rapid and simple Au electrodeposition.

To further estimate the immobilization content (e.g. density, Γss) of dSH-HP in depAu/GCE, we also recoded the chronocoulometry (CC) signal of the modified electrode dSH-HP/depAu/GCE in 10 mM Tris-HCl (pH 7.4) without and with RuHex as electron mediator [32]. By scanning from 0 to 0.5 s, the plotted curves between the charges (Q) *vs.* the square root of scan time ($t^{1/2}$) were shown in Fig. 2B. Two intercepts at t = 0 respectively corresponded to the total charge (Q_{total}) in the presence of RuHex and the double-layer charge (Q_{dl}) in the absence of RuHex,

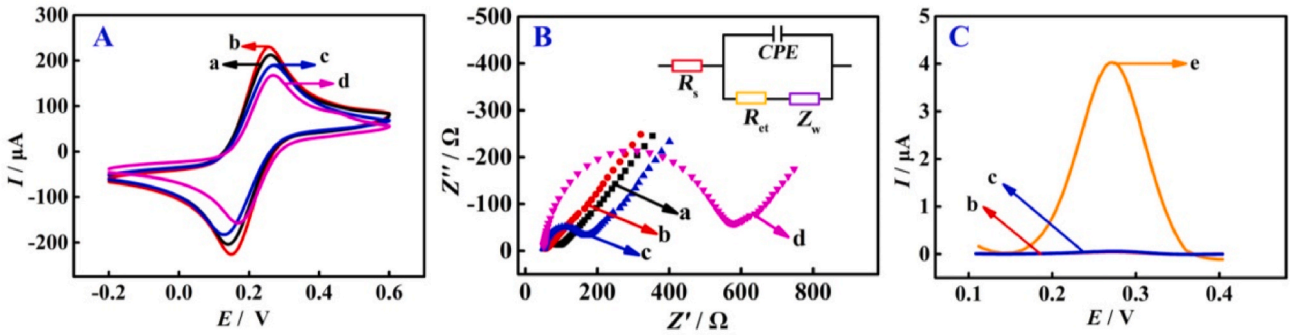

Fig. 1. (A) CV and (B) EIS signals of stepwise modified electrodes in $[Fe(CN)_6]^{3-/4-}$ (pH 7.4): (a) GCE, (b) depAu/GCE, (c) dSH-HP/depAu/GCE, and (d) GOx-ES1+HRP-ES2/dSH-HP/depAu/GCE without the conjugation of Fc (the inset is the fitted Randle equivalent circuit). (C) SWV response measured in PBS (pH 7.0) containing glucose (4 mM): (b) depAu/GCE, (c) dSH-HP/depAu/GCE, and (e) GOx-ES1+Fc@ HRP-ES2/dSH-HP/depAu/GCE.

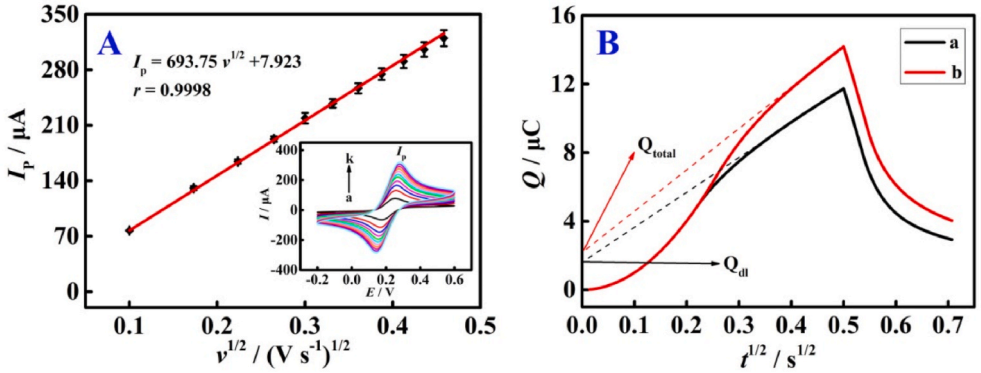

Fig. 2. (A) Linear correlation plotted by the anodic peak current (I_p, μA) *vs.* $\nu^{1/2}$ (Inset is CV signal of depAu/GCE measured in $[Fe(CN)_6]^{3-/4-}$ (pH 7.4) at different ν: a-k, 0.01, 0.03, 0.05, 0.07, 0.09, 0.11, 0.13, 0.15, 0.17, 0.19 and 0.21 V·s^{-1}). (B) Chronocoulometry signal of dSH-HP/depAu/GCE in 10 mM Tris-HCl (pH 7.4) before (a) and after (b) adding 50 μM RuHex. Error bars: standard deviation (*s*), $n = 5$.

respectively. So, the surface-confined ssDNA charge ($Q_{ss} = Q_{total}$-Q_{dl}) in the electrode sensing interface can be easily obtained. In this case, the density Γss of dSH-HP immobilized in depAu/GCE was estimated using the equation of $\Gamma ss = [(Q_{ss}N_A)/(nFA)](z/m)$ [33], where N_A and F are Avogadro constant and Faraday constant, $z = 3$ is the charge of RuHex, and $m = 56$ is the nucleotide number of dSH-HP. Based on all the obtained data, the Γss discussed here was calculated to be about 9.8×10^{11} molecules·cm^{-2}, demonstrating that a large amount of dSH-HP can be highly efficiently conjugated in depAu/GCE via dual Au–S bonds. As expected, all the immobilized dSH-HP might self-adopt a more compact style with stronger binding capability [27], which would facilitate the subsequent combination of two enzyme strands to orient a functional DNA nanostructure for confining GOx and HRP.

3.4. Verification of no non-specific blockers passivation

Benefited from this subtle design, the high specificity of the developed biosensor was maintained without using non-specific absorption blockers for the electrode surface passivation. We compared the SWV signal by adding aDNA (100 pM) in the human serum samples before and after incubating the blocker MCH. From Fig. 3A and B, no significant difference of SWV currents without and with MCH was observed, suggesting that non-specific blockers were unnecessary in this detection system. This might be attributed to such a fact that the stable upright hairpin conformation of dSH-HP was highly specific and responsive to orient the Y-shaped structure for bienzymatic cascade catalysis. In principle, no treatment and occupation of blocking small molecules in electroactive sensing surface were more advantageous to minimize the background interference.

3.5. Demonstration of bienzymatic cascade catalysis

In this work, the electrochemical signal amplification was implemented by two sequential cascade reactions involving in GOx and HRP. The most efficient catalysis might be relied on the harmonization of glucose, GOx and HRP, as well as the suitable spatial distance for the catalytic substrate transfer. Under the optimized conditions, we monitored the SWV response in the absence of glucose, GOx and/or HRP. From Fig. 4A, much lower SWV peak currents were observed without glucose, GOx or HRP in the detection system, demonstrating the utility of cascade reaction to promote the electron transfer and enhance the electrochemical signal. Of note, the absence of HRP caused no SWV response, because of the disabled conjugation of Fc in ES2 without HRP as a bridge. Furthermore, we explored the cascade efficiency influenced by different spatial distances of GOx and HRP. By changing the T base numbers tethered in ES1 close to 3' end (Table S1), the SWV current gradually went up and went down at 4 of T (Fig. 4B). Based on the model of Y-shaped structure, T numbers of 0–12 in ES1 corresponded to the spatial distance of 7.8 nm–11.9 nm roughly estimated by totalizing the base sequence (23- to 35-nt) of GOx-conjugated ES1 and HRP-conjugated ES2. Similar to those results reported in other cascade strategies, the most efficient catalysis in our study was occurred at approximately 9.1 nm (ES1 with T_4) of spatial distance between GOx and HRP, while it was disabled at shorter or longer distance than 9.1 nm. This might originate from the crowding effect at a smaller distance or the invalid diffusion of the intermediate product at a bigger distance [12–14].

3.6. Analytical performance of the electrochemical biosensor

By introducing different concentrations of aDNA in the detection

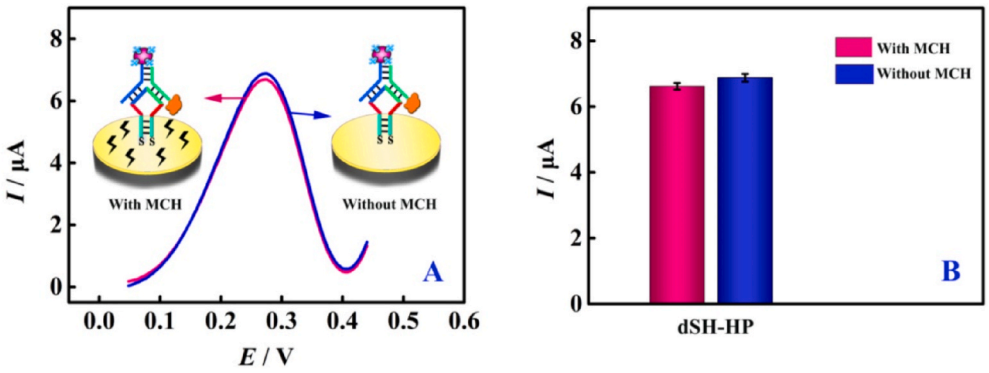

Fig. 3. (A and B) SWV responses of different electrodes with MCH and without MCH as non-specific blocker for passivation. Error bars: *s*, $n = 5$.

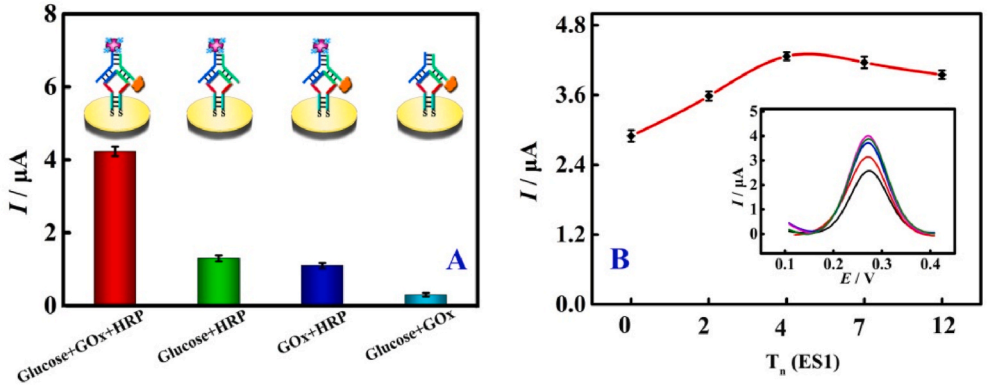

Fig. 4. The SWV responses of Fc on different electrodes (A) in the absence of glucose, GOx or HRP, and (B) using different ES1 tethering different numbers of T base (T_n) close to 3′ end. Error bars: *s*, $n = 5$.

system under the optimal conditions, the SWV response was measured in PBS (pH 7.0) with 4 mM glucose. Apparently, the SWV signal gradually increased with the rising of aDNA and reached to the highest at 10 nM (Fig. 5A). With the difference (ΔI) of the corresponding peak current deducting that of the Blank, the calibration curve was plotted in response to the logarithm of aDNA concentrations ($\lg c_{aDNA}$) in the range of 0.5 fM to 10 nM (Fig. 5B). A good linear relationship ($\Delta I = 1.135\lg c_{aDNA}+4.164$) was obtained with a correlation coefficient (r) of 0.9974. The limit of detection (LOD) was evaluated according to $\Delta I_L = \Delta I_0 + k s_B$ recommended by IUPAC [34], where ΔI_0 is the SWV peak of the background and s_B is its standard deviation, and the coefficient k equals three to allow a confidence level of 99.9%. By using ΔI_L (μA) obtained from the average ΔI_0 and s_B of five parallel measurements, LOD was calculated to be 0.22 fM. From Table S2, our biosensor was comparable with or superior to some reported methodologies for the electrochemical detection of different DNAs.

3.7. Stability, repeatability, specificity and regeneration

Under the optimal experimental conditions, five modified electrodes were prepared in one-batch and five-batch using 100 fM of aDNA. After the five electrodes in one-batch were stored for 4, 8, 12 and 16 days, the SWV currents retained 97.9%, 95.6%, 92.7% and 90.3% of the initial values (Fig. 6A). When compared the SWV signals with those in five-batch, the relative standard deviation (RSD) of 3.5% for inter-assay and 4.2% of intra-assay were obtained (Fig. 6B). Moreover, by using M1-aDNA, M2-aDNA and M3-aDNA as interferents, the specificity of our biosensor was investigated by measuring the SWV response to aDNA (100 fM) under the same experiment conditions. The obtained results in Fig. 6C indicated a satisfactory selectivity because the SWV currents caused by these interferents (10 pM), almost the same as that of the Blank, were much lower than aDNA. All the observations revealed our electrochemical biosensor was stable, repeatable and specific.

Due to the one-step assembly of the functional DNA structure for bienzymatic cascade catalysis, our biosensor might be renewable by using a competitive strand (**C***) to take off Fc@HRP-ES2 via complementary hybridization. Fig. 6D displayed the SWV currents of five electrodes before and after repeatedly treated with **C*** and Fc@HRP-ES2 for six times. Obviously, the treatment led to the sharply decreasing of SWV currents, indicating the absence of GOx-ES1 and redox-active Fc in the electrode sensing interface and disabled cascade catalysis due to the disassembly of Y-shaped structure. When introducing Fc@HRP-ES2 once again in the resultant electrode surface, the SWV signal could recover to 90.2% of the initial value after six repeated recycles, demonstrating the good regeneration of our biosensor.

3.8. Recovery in human serum samples

By using the standard addition method, we investigated the recovery of aDNA in the clinical human serum samples kindly provided by the Army Medical University, Xinqiao Hospital (Chongqing, China). Different concentrations of aDNA (10 fM to 1 nM) were spiked into the serum samples. After undergoing the stepwise fabricating process, the SWV signal of our biosensor was measured in PBS (pH 7.0) containing 4 mM of glucose. Based on the above linear equation, the recoveries of aDNA in these serums were obtained as 90.7%–108% with RSD from 2.1% to 4.6% (Table S3), suggesting the preliminary applicability of this electrochemical protocol in real samples.

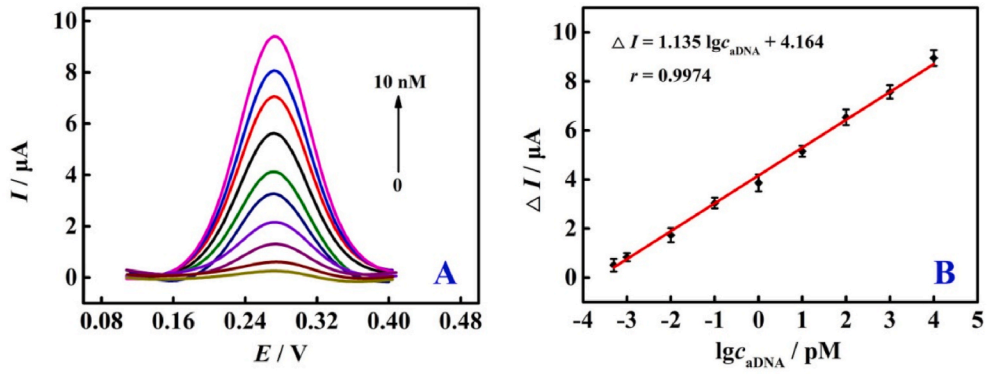

Fig. 5. (A) SWV responses of our biosensor for different concentrations of aDNA: 0, 0.5, 1, 10, 100 fM, 1, 10, 100 pM, 1 and 10 nM. (B) The resultant linear calibration curve plotted by the SWV peak current of Fc deducting the Blank (ΔI, μA) *vs.* the logarithm of aDNA concentration ($\lg c_{aDNA}$). Error bars: *s*, $n = 5$.

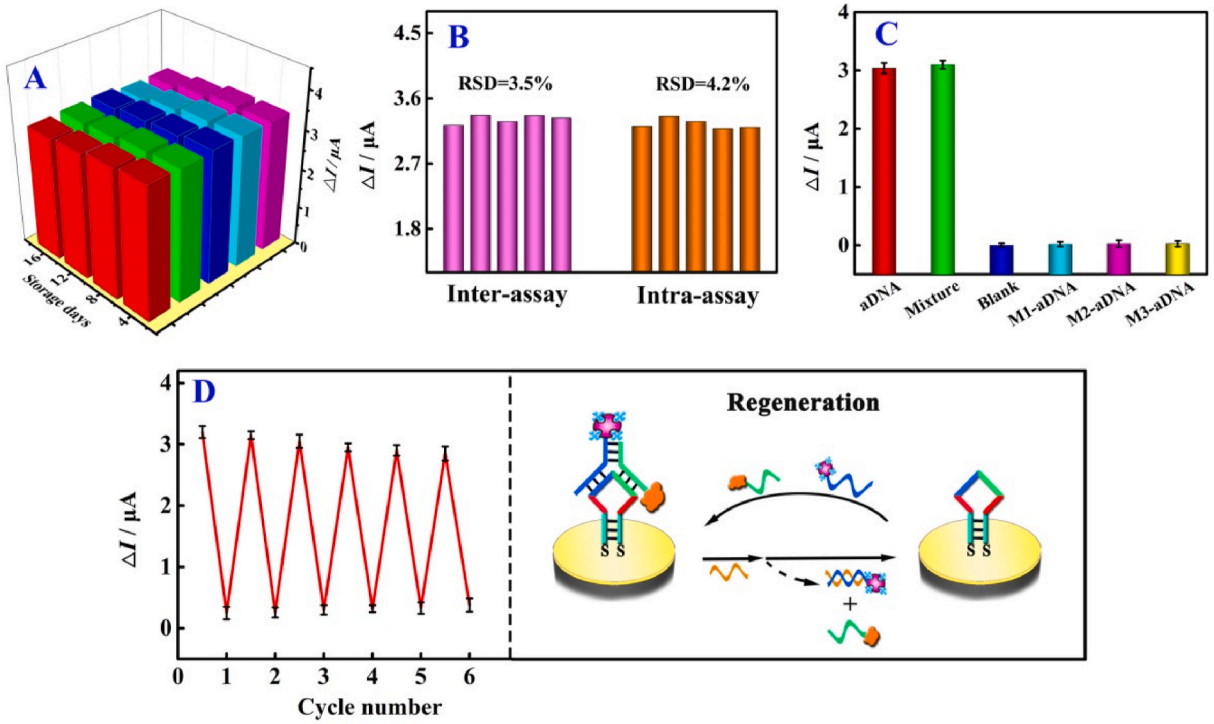

Fig. 6. SWV responses of different biosensors: (A) after stored for 4, 8, 12 and 16 days, (B) prepared in one-batch (inter-assay) and five-batch (intra-assay), and (C) responsive to aDNA (100 fM) against Blank, M1-aDNA, M2-aDNA, and M3-aDNA with the same concentration of 10 pM. (D) SWV responses for repeated re-generations, and the schematic regeneration of the biosensor. Error bars: *s*, $n = 5$.

4. Conclusions

In conclusion, we developed a simple and renewable electrochemical biosensor for determining sequence-specific biomarker DNA with the fM detection limit. The innovative recognition and amplification fashion relied on the unique design of dSH-HP as a capture probe and the highly efficient bienzymatic cascade catalysis confined in a dSH-HP-oriented Y-shaped DNA structure. Especially, the paired stem of dSH-HP was acted as a rigid scaffold to keep it adopting proper upright and compact conformation in the electrode surface. Importantly, the unpaired loop as an enclosed binding platform could capture two enzyme strands, which were chemically conjugated with GOx and Fc-modified HRP. The former was dependently released from ExoIII-cleaved recycling in response to the target aDNA. In this assembled functional DNA structure, the cascade reaction was continuously driven by GOx-catalyzed oxidization of glucose, in situ generating H_2O_2, and simultaneously HRP catalyzed the decomposition of the resultant H_2O_2, significantly promoting the electron transfer of Fc oxidization. The obtained results demonstrated the detection feasibility and reliability of this sensitive, specific and renewable strategy, being a great promise to provide a new paradigm for biosensing and bioanalysis. Nonetheless, in the future exploring more elaborate DNA architectures would be desired to facilitate the efficient electron transfer of Fc as redox mediator.

Author contribution

Jiaxi Gao: Conceptualization, Methodology, Software, Data curation, Writing-Original draft preparation; **Xiaoyu Hua**: Visualization, Software, Investigation, Writing-Original draft preparation; **Ruo Yuan**: Supervision, Writing-Reviewing; **Qiong Li**: Supervision and Editing; **Wenju Xu**: Supervision, Writing-Reviewing and Editing, Validation.

Declaration of competing interest

The authors declare that they have no known competing financial interests or personal relationships that could have appeared to influence the work reported in this paper.

Acknowledgements

We really appreciate the financial support of the National Natural Science Foundation of China (NNSF) of China (21775123 and 21775124) and the Natural Science Foundation Project of Chongqing (cstc2018jcyjAX0214) to this work.

Appendix A. Supplementary data

Supplementary data to this article can be found online at https://doi.org/10.1016/j.talanta.2021.122643.

References

[1] J.L. Fu, Y.R. Yang, S. Dhakal, Z. Zhao, M.H. Liu, T. Zhang, N.G. Walter, H. Yan, Assembly of multienzyme complexes on DNA nanostructures, Nat. Protoc. 11 (2016) 2243–2273.
[2] Z. Zhao, J.L. Fu, S. Dhakal, A. Johnson-Buck, M.H. Liu, T. Zhang, N.W. Woodbury, Y. Liu, N.G. Walter, H. Yan, Nanocaged enzymes with enhanced catalytic activity and increased stability against protease digestion, Nat. Commun. 7 (2016) 10619–10627.
[3] S.H. Kim, K.R. Kim, D.R. Ahn, J.E. Lee, E.G. Yang, S.Y. Kim, Reversible regulation of enzyme activity by pH-responsive encapsulation in DNA nanocages, ACS Nano 11 (2017) 9352–9359.
[4] W.H. Chen, M. Vázquez-González, A. Zoabi, R. Abu-Reziq, I. Willner, Biocatalytic cascades driven by enzymes encapsulated in metal-organic framework nanoparticles, Nat. Catal. 1 (2018) 689–695.
[5] E. Kim, P.D. Howes, S.W. Crowder, M.M. Stevens, Multi-amplified sensing of microRNA by a small DNA fragment-driven enzymatic cascade reaction, ACS Sens. 2 (2017) 111–118.
[6] W.P. Klein, R.P. Thomsen, K.B. Turner, S.A. Walper, J. Vranish, J. Kjems, M. G. Ancona, I.L. Medintz, Enhanced catalysis from multienzyme cascades assembled on a DNA origami triangle, ACS Nano 13 (2019) 13677–13689.
[7] L. Li, Y. Zhang, Z. Yan, M.Q. Chen, L.N. Zhang, P.N. Zhao, J.H. Yu, Ultrasensitive photoelectrochemical detection of microRNA on paper by combining a cascade nanozyme- engineered biocatalytic precipitation reaction and target-triggerable DNA motor, ACS Sens. 5 (2020) 1482–1490.

[8] T.A. Ngo, E. Nakata, M. Saimura, T. Morii, Spatially organized enzymes drive cofactor- coupled cascade reactions, J. Am. Chem. Soc. 138 (2016) 3012–3021.
[9] G.R. Chado, M.P. Stoykovich, J.L. Kaar, Role of dimension and spatial arrangement on the activity of biocatalytic cascade reactions on scaffolds, ACS Catal. 6 (2016) 5161–5169.
[10] F. Wang, C.H. Lu, I. Willner, From cascaded catalytic nucleic acids to enzyme-DNA nanostructures: controlling reactivity, sensing, logic operations, and assembly of complex structures, Chem. Rev. 114 (2014) 2881–2941.
[11] J.L. Lin, L. Palomec, I. Wheeldon, Design and analysis of enhanced catalysis in scaffolded multienzyme cascade reactions, ACS Catal. 4 (2014) 505–511.
[12] B.B. Kou, Y.Q. Chai, Y.L. Yuan, R. Yuan, Dynamical regulation of enzyme cascade amplification by a regenerated DNA nanotweezer for ultrasensitive electrochemical DNA detection, Anal. Chem. 90 (2018) 10701–10706.
[13] D. Wang, Y.Q. Chai, Y.L. Yuan, R. Yuan, Precise regulation of enzyme cascade catalytic efficiency with DNA tetrahedron as scaffold for ultrasensitive electrochemical detection of DNA, Anal. Chem. 91 (2019) 3561–3566.
[14] L.Q. Kong, D. Wang, Y.Q. Chai, Y.L. Yuan, R. Yuan, Electrocatalytic efficiency regulation between target-induced HRP-mimicking DNAzyme and GOx with low background for ultrasensitive detection of thrombin, Anal. Chem. 91 (2019) 10289–10294.
[15] H.M. Meng, H. Liu, H. Kuai, R. Peng, L. Mo, X.B. Zhang, Aptamer-integrated DNA nanostructures for biosensing, bioimaging and cancer therapy, Chem. Soc. Rev. 45 (2016) 2583–2602.
[16] D.N. Wang, R. Guo, Y.Y. Wei, Y.Z. Zhang, X.Y. Zhao, Z.R. Xu, Sensitive multicolor visual detection of telomerase activity based on catalytic hairpin assembly and etching of Au nanorods, Biosens. Bioelectron. 122 (2018) 247–253.
[17] Y.H. Yang, Y.G. Fu, H.L. Su, L. Mao, M. Chen, Sensitive detection of MCF-7 human breast cancer cells by using a novel DNA-labeled sandwich electrochemical biosensor, Biosens. Bioelectron. 122 (2018) 175–182.
[18] C. Feng, T.S. Chen, D.S. Mao, F. Zhang, B. Tian, X.L. Zhu, Construction of a ternary complex based DNA logic nanomachine for a highly accurate imaging analysis of cancer cells, ACS Sens. 5 (2020) 3116–3123.
[19] E.H. Xiong, X.H. Zhang, Y.Q. Liu, J.W. Zhou, P. Yu, X.Y. Li, J.H. Chen, Ultrasensitive electrochemical detection of nucleic acids based on the dual-signaling electrochemical ratiometric method and exonuclease III-assisted target recycling amplification strategy, Anal. Chem. 87 (2015) 7291–7296.
[20] Y. Zhang, Y.N. Deng, C.S. Wang, L.D. Li, L.D. Xu, Y.J. Yu, X. Su, Single-molecule dynamic DNA junctions for engineering robust molecular switches, Chem. Sci. 10 (2019) 5959–5966.
[21] E.H. Xiong, Z.Z. Li, X.H. Zhang, J.W. Zhou, X.X. Yan, Y.Q. Liu, J.H. Chen, Triple-helix molecular switch electrochemical ratiometric biosensor for ultrasensitive detection of nucleic acids, Anal. Chem. 89 (2017) 8830–8835.
[22] C.X. Zhu, M.Y. Liu, X.H. Zhang, J.H. Chen, A new electrochemical aptasensor for sensitive assay of a protein based on the dual-signaling electrochemical ratiometric method and DNA walker strategy, Chem. Commun. 54 (2018) 10359–10362.
[23] J. Zheng, N.X. Li, C.R. Li, X.X. Wang, Y.C. Liu, G.B. Mao, X.H. Ji, Z.K. He, A nonenzymatic DNA nanomachine for biomolecular detection by target recycling of hairpin DNA cascade amplification, Biosens. Bioelectron. 107 (2018) 40–46.
[24] K. Zhang, J.X. Cao, Y.X. Wu, F.T. Hu, T.H. Li, Y. Wang, N. Gan, A fluorometric aptamer method for kanamycin by applying a dual amplification strategy and using double Y-shaped DNA probes on a gold bar and on magnetite nanoparticles, Microchim. Acta 186 (2019) 120–128.
[25] H. He, J. Dai, Z. Duan, Y. Meng, C. Zhou, Y. Long, B. Zheng, J. Du, Y. Guo, D. Xiao, Target-catalyzed autonomous assembly of dendrimer-like DNA nanostructures for enzyme- free and signal amplified colorimetric nucleic acids detection, Biosens. Bioelectron. 86 (2016) 985–989.
[26] J. Li, Q. Liu, H. Xi, X. Wei, Z. Chen, Y-shaped DNA duplex structure-triggered gold nanoparticle dimers for ultrasensitive colorimetric detection of nucleic acid with the dark-field microscope, Anal. Chem. 89 (2017) 12850–12856.
[27] C. Li, D. Wu, X.L. Hu, Y. Xiang, Y.Q. Shu, G.X. Li, One-step modification of electrode surface for ultrasensitive and highly selective detection of nucleic acids with practical applications, Anal. Chem. 88 (2016) 7583–7590.
[28] E.H. Xiong, Z.Z. Li, X.H. Zhang, J.W. Zhou, X.X. Yan, Y.Q. Liu, J.H. Chen, Triple-helix molecular switch electrochemical ratiometric biosensor for ultrasensitive detection of nucleic acids, Anal. Chem. 89 (2017) 8830–8835.
[29] X.Y. Hua, E.F. Yang, W.T. Yang, R. Yuan, W.J. Xu, LAMP-generated H^+ ions-induced dimer i-motif as signal transducer for ultrasensitive electrochemical detection of DNA, Chem. Commun. 55 (2019) 12463–12466.
[30] R. Mukherjee, R. Krishnan, T.M. Lu, N. Koratkar, Nanostructured electrodes for high- power lithium ion batteries, Nanomater. Energy 1 (2012) 518–533.
[31] C.X. Guo, X.T. Zheng, Z.S. Lu, X.W. Lou, C.M. Li, Biointerface by cell growth on layered graphene-artificial peroxidase-protein nanostructure for in situ quantitative molecular detection, Adv. Mater. 22 (2010) 5164–5167.
[32] J. Zhang, S.P. Song, L.H. Wang, D. Pan, C.H. Fan, A gold nanoparticle-based chronocoulometric DNA sensor for amplified detection of DNA, Nat. Protoc. 2 (2007) 2888–2895.
[33] X.L. Zhang, Z.H. Yang, Y.Y. Chang, D. Liu, Y.R. Li, Y.Q. Chai, Y. Zhuo, R. Yuan, Programmable mismatch-fueled high-efficiency DNA signal converter, Chem. Sci. 11 (2020) 148–153.
[34] G.L. Long, J.D. Winefordner, Limit of detection. A closer look at the IUPAC definition, Anal. Chem. 55 (1983) 712A–724A.